

Speedy-Splat: Fast 3D Gaussian Splatting with Sparse Pixels and Sparse Primitives

Alex Hanson Allen Tu Geng Lin Vasu Singla
Matthias Zwicker Tom Goldstein

University of Maryland, College Park

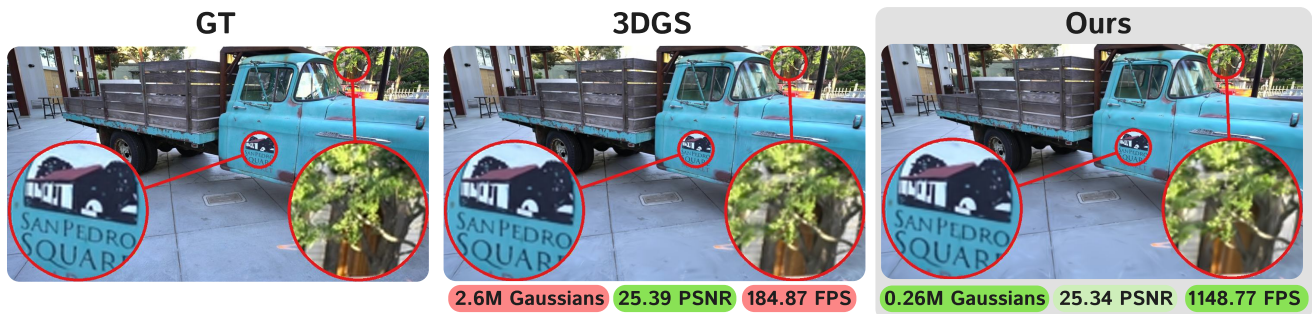


Figure 1. We reduce the number of Gaussians by over 90%, only marginally decrease PSNR, and accelerate rendering speed by $6.2\times$ in the Tanks & Temples truck scene when compared to 3D Gaussian Splatting (3D-GS). Additionally, we speed up training time by $1.38\times$.

Abstract

3D Gaussian Splatting (3D-GS) is a recent 3D scene reconstruction technique that enables real-time rendering of novel views by modeling scenes as parametric point clouds of differentiable 3D Gaussians. However, its rendering speed and model size still present bottlenecks, especially in resource-constrained settings. In this paper, we identify and address two key inefficiencies in 3D-GS, achieving substantial improvements in rendering speed, model size, and training time. First, we optimize the rendering pipeline to precisely localize Gaussians in the scene, boosting rendering speed without altering visual fidelity. Second, we introduce a novel pruning technique and integrate it into the training pipeline, significantly reducing model size and training time while further raising rendering speed. Our Speedy-Splat approach combines these techniques to accelerate average rendering speed by a drastic $6.71\times$ across scenes from the Mip-NeRF 360, Tanks & Temples, and Deep Blending datasets with $10.6\times$ fewer primitives than 3D-GS.

1. Introduction

Fast rendering of photorealistic novel views has been a long-standing goal in computer vision and graphics. Neural Radiance Fields (NeRF) [20] and its variants have made sig-

nificant strides in photorealistic 3D scene reconstruction by representing scenes as continuous neural volumetric models that encode scene density and color at spatial coordinates. However, despite recent efforts [4, 21, 24], fast rendering in NeRF remains a challenge, as the volumetric sampling used in ray-marching is computationally expensive. Recently, 3D Gaussian Splatting (3D-GS) [14] has emerged as a promising alternative that enables real-time rendering by modeling scenes as parametric point clouds of differentiable 3D Gaussians. Nevertheless, its rendering speed is still limited in practice by high parameter counts and certain algorithmic inefficiencies. Efficient rendering is essential in settings like virtual reality, networked applications, and multi-view streaming, and real-time rendering on resource-constrained edge devices like mobile phones is yet to be achieved [18].

Although recent works on compressing 3D-GS models [6, 7, 11, 22] achieve some speed-ups by reducing the number of parameters, few approaches directly target rendering speed [8, 18]. In this paper, we specifically address this gap by demonstrating that the rendering speed of 3D-GS models can be drastically increased while maintaining competitive image quality. Additionally, we show that our methods reduce training time and substantially decrease model size.

We begin by observing that the cost of 3D-GS rendering is proportional to both the number of Gaussians in the scene

and the number of pixels processed per Gaussian. Our approach optimizes both factors. First, we reduce the number of pixels that are processed for each Gaussian by accurately localizing it in the rendered image. Second, we reduce the total number of Gaussians in the model through a novel approach that maintains rendering quality.

3D-GS implements tile rendering to localize Gaussians in the image plane, assigning them to only the image tiles that they intersect. We find the existing algorithm to be overly conservative; in Section 4.1.1, we address this by introducing our SnugBox algorithm to precisely localize Gaussians by computing a tight bounding box around their extent. Then, in Section 4.1.2, we extend SnugBox with our AccuTile algorithm to identify exact tile intersections. Both approaches are plug-and-play, lead to respective inference speed-ups of $1.82\times$ and $1.99\times$ on average, and do not change the 3D-GS renderings.

To reduce model size while preserving visual fidelity, we reduce the memory requirement of an existing pruning method [11] by $36\times$ and simplify its integration into the 3D-GS training pipeline. Gaussians are replicated and pruned at regular intervals during the densification stage of 3D-GS training. In Section 4.2.2, we augment the densification stage with our Soft Pruning method to prune 80% of Gaussians at regular intervals. After the densification stage is completed, we use our Hard Pruning method, described in Section 4.2.3, to prune an additional 30% of Gaussians at set intervals.

Our Speedy-Splat approach integrates both techniques into the 3D-GS training pipeline. On average, rendering speed is accelerated by $6.71\times$, model size is reduced by $10.6\times$, and training speed is improved by $1.4\times$ across all evaluated scenes while maintaining high image quality.

In summary, we propose the following contributions:

1. **SnugBox**: A precise algorithm for computing Gaussian-tile bounding box intersections.
2. **AccuTile**: An extension of SnugBox for computing exact Gaussian-tile intersections.
3. **Soft Pruning**: An augmentation for pruning Gaussians during densification.
4. **Hard Pruning**: An augmentation for pruning Gaussians post-densification.

2. Related work

The real-time rendering speed of 3D-GS [14] on desktop GPUs has sparked research interest in further accelerating its training and inference in resource-constrained environments. In this section, we discuss several related works that have emerged in the literature.

2.1. Pruning

A large portion of Gaussians in vanilla 3D-GS models are redundant [6, 7, 22], motivating a recent line of

work focused on pruning Gaussians from 3D-GS models to boost rendering speed with minimal loss of visual fidelity [1, 2, 6, 7, 10, 11, 17, 18, 22]. Nearly all approaches assign a significance score to each Gaussian that is used to rank and prune them. Several works compute the aggregated ray contribution for each Gaussian across all input images [6, 7, 17, 22], while others combine opacity with additional information, such as gradients per Gaussian, to calculate their pruning criterion [1, 2, 19]. Papantonakis et al. [23] use resolution and scale-aware redundancy metrics, EA-GLES [10] calculates the total transmittance per Gaussian, and Lin et al. [18] accelerate inference speed through an efficiency-aware strategy and foveated rendering.

PUP 3D-GS [11] introduces a more principled approach by deriving a Hessian for each Gaussian that represents its sensitivity to the reconstruction error. While PUP 3D-GS achieves state-of-the-art post-hoc pruning results, computing its sensitivity score incurs considerable storage requirements that limit its viability for use during training. Our pruning approach directly extends PUP 3D-GS by improving its memory efficiency by $36\times$.

2.2. Other Methods

In addition to pruning, several other strategies have been explored to enhance the rendering and training speed of 3D-GS. Mini-Splatting [7] modifies its densification strategies and adds a simplification stage to constrain the number of Gaussians. 3DGS-LM [13] replaces Adam [15] with a tailored Levenberg-Marquardt optimizer [9]. Taming 3DGS [25] proposes a constructive optimization process that limits the number of Gaussians to a pre-defined threshold set by the user. DISTWAR [5] dives into the low-level implementation of GPU thread scheduling and optimizes atomic processing with a novel primitive. FlashGS [8] is a recent concurrent work that also uses efficient tile intersection to improve rendering speed; however, their overall speedup is lower than ours because they do not explore pruning. Most of these approaches are orthogonal to ours and can be applied alongside it.

3. Background

3.1. 3D Gaussian Splatting Overview

3D Gaussian Splatting (3D-GS) [14] models scenes as parametric, point-based representations that use differentiable 3D Gaussians as primitives. Given a set of ground truth training images $\mathcal{I}_{gt} = \{\mathbf{I}_i \in \mathbb{R}^{H \times W}\}_{i=1}^K$, the scene is initialized by using Structure from Motion (SfM) to produce a sparse point cloud that serves as the initial means for the 3D Gaussians. The estimated camera poses $\mathcal{P}_{gt} = \{\phi_i \in \mathbb{R}^{3 \times 4}\}_{i=1}^K$ are paired with their corresponding images and are used to optimize the scene.

Each 3D Gaussian primitive \mathcal{G}_i is parameterized by three

Table 1. Average execution time (milliseconds) of each function across all scenes. The operation in each row is applied **cumulatively** to all of the following rows. For each model, accurate measurements are collected by averaging execution times across three runs that each render the test set 20 times to reduce variance. The **fastest** and **second** fastest times are color coded.

| Method | Preprocess | Inclusive Sum | Duplicate with Keys | Radix Sort | Identify Tile Ranges | Render | Overall |
|---------------|----------------|----------------|---------------------|----------------|----------------------|----------------|----------------|
| Baseline | 0.665 | 0.045 | 0.570 | 1.551 | 0.082 | 4.483 | 7.478 |
| +SnugBox | 0.656 | 0.046 | 0.208 (2.738×) | 0.729 (2.126×) | 0.041 (1.980×) | 2.344 (1.913×) | 4.102 (1.823×) |
| +AccuTile | 0.668 | 0.046 | 0.221 (2.575×) | 0.612 (2.533×) | 0.035 (2.326×) | 2.062 (2.175×) | 3.748 (1.995×) |
| +Soft Pruning | 0.370 (1.798×) | 0.030 (1.494×) | 0.146 (3.906×) | 0.404 (3.843×) | 0.024 (3.422×) | 1.337 (3.354×) | 2.381 (3.141×) |
| +Hard Pruning | 0.091 (7.293×) | 0.016 (2.769×) | 0.090 (6.325×) | 0.215 (7.217×) | 0.013 (6.537×) | 0.619 (7.247×) | 1.114 (6.712×) |

geometry parameters – mean $\mu_i \in \mathbb{R}^3$, scale $s_i \in \mathbb{R}^3$, and rotation $r_i \in \mathbb{R}^4$ – and two color parameters – view-dependent spherical harmonics $h_i \in \mathbb{R}^{16 \times 3}$ and opacity $\sigma_i \in \mathbb{R}$. The set of all parameters can be described as:

$$\mathcal{G} = \{\mathcal{G}_i = \{\mu_i, s_i, r_i, h_i, \sigma_i\}\}_{i=1}^N, \quad (1)$$

where N is the number of Gaussians in the model.

Given camera pose ϕ , the scene is rendered by projecting all Gaussians to image space and applying alpha blending to each pixel. Models are optimized via stochastic gradient descent on image reconstruction losses:

$$L(\mathcal{G}|\phi, I_{gt}) = \|I_{\mathcal{G}}(\phi) - I_{gt}\|_1 + L_{D-SSIM}(I_{\mathcal{G}}(\phi), I_{gt}), \quad (2)$$

where $I_{\mathcal{G}(\phi)}$ is the rendered image for pose ϕ .

During optimization, the scene is periodically densified by cloning and splitting uncertain Gaussians and pruned by removing large and transparent Gaussians. The opacities of the Gaussians are also periodically reset.

3.2. 3D Gaussian Splatting Rendering Specifics

3D-GS uses a tile-based rendering strategy that divides the rendered image into 16×16 pixel tiles. Each Gaussian is projected into image space, where its intersection with these tiles is computed. Then, these Gaussian-to-tile mappings are sorted to collect and order the Gaussians by depth for pixel-wise rendering.

Rendering runtime is dominated by six key functions. Table 1 empirically analyzes the execution time of each function and highlights the improvements achieved by our methods. Descriptions of each function are provided in the following sections.

3.2.1. Preprocessing

The `preprocess` kernel is parallelized such that each thread processes a single Gaussian \mathcal{G}_i . It computes a 2D projection of \mathcal{G}_i to image space and obtains a count of tiles that it intersects.

The mean μ_i is projected to image space using a view-ing transform \mathbf{W} and a perspective projection, yielding 2D mean $\mu_{i_{2D}}$ and depth that are stored for later processing. The scale s_i and rotation r_i parameters are converted to the

diagonal scale \mathbf{S}_i and rotation \mathbf{R}_i matrices. The 3D covariance is then defined as:

$$\Sigma_{i_{3D}} = \mathbf{R}_i \mathbf{S}_i \mathbf{S}_i^T \mathbf{R}_i^T, \quad (3)$$

which is projected via:

$$\hat{\Sigma}_{i_{3D}} = \mathbf{J} \mathbf{W} \Sigma_{i_{3D}} \mathbf{W}^T \mathbf{J}^T, \quad (4)$$

where \mathbf{J} is the Jacobian of the first order approximation of the perspective projection. Dropping the last row and column of $\hat{\Sigma}_{i_{3D}}$ gives $\Sigma_{i_{2D}}$ [14, 26]. The largest eigenvalue of $\Sigma_{i_{2D}}$ is used to compute the count of tiles intersected by this Gaussian \mathcal{G}_i as shown in Figure 2a. $\Sigma_{i_{2D}}^{-1}$ is computed, and a view dependent color c_i is derived from \mathbf{W} and h_i . All three values are stored for later processing.

3.2.2. Sorting

After preprocessing, four functions process the Gaussians for pixel-wise rendering:

- **InclusiveSum:** A CUDA primitive that computes the prefix sum over all Gaussian-tile counts to allocate key and value arrays for Gaussian-to-tile mapping.
- **duplicateWithKeys:** A Gaussian-parallel kernel that recomputes Gaussian-tile intersections to generate a key for each intersecting tile, consisting of the tile index and Gaussian depth.
- **RadixSort:** A CUDA primitive that sorts the key array, ordering Gaussian indices by tile and then depth.
- **identifyTileRanges:** A kernel parallelized across the key array to post-process keys before pixel rendering.

3.2.3. Rendering

The `render` kernel is parallelized across pixels. For each pixel p , all Gaussians within its corresponding tile are loaded and processed in depth order as determined by `RadixSort`. An alpha value:

$$\alpha_i(p) = \sigma_i g_i(p) \quad (5)$$

is computed for each Gaussian \mathcal{G}_i , where g_i is the value of the projected 2D Gaussian at pixel p :

$$g_i = e^q, q = -\frac{1}{2}(p - \mu_{i_{2D}}) \Sigma_{i_{2D}}^{-1} (p - \mu_{i_{2D}})^T. \quad (6)$$

If $\alpha_i > \frac{1}{255}$, then the Gaussian is included in the alpha compositing of the pixel color C , given by:

$$C(p) = \sum_{i \in \mathcal{N}} c_i \alpha_i(p) \prod_{j=1}^{i-1} (1 - \alpha_j(p)). \quad (7)$$

4. Methods

Our Speedy-Splat methods are motivated by two key insights into inefficiencies within the 3D-GS rendering pipeline. First, Gaussian Splatting grossly overestimates the extent of Gaussians in the image. Second, as demonstrated by [11] and other recent pruning works, 3D-GS models are heavily overparameterized.

4.1. Precise Tile Intersect

Gaussian Splatting identifies tiles intersected by Gaussian \mathcal{G}_i by calculating the maximum eigenvalue λ_{\max} of its projected 2D covariance $\Sigma_{i_{2D}}$, then selecting all tiles that intersect the square inscribing the circle defined by center $\mu_{i_{2D}}$ and radius:

$$r = \lceil 3\sqrt{\lambda_{\max}} \rceil. \quad (8)$$

This approach neglects opacity σ_i in its calculation and generally overestimates the Gaussian extent, as illustrated by Figure 2a. The actual extent of Gaussian \mathcal{G}_i , shown in Figure 2b, is given by the threshold placed on its alpha value α_i . Specifically, \mathcal{G}_i does not contribute to the rendering of pixel p if $\alpha_i < \frac{1}{255}$ for p . By applying the actual extent in tile intersection calculations, we arrive at a far more concise set of intersected tiles.

We now show the derivation of this extent. The furthest pixel extent of Gaussian \mathcal{G}_i can be determined by directly substituting this threshold into Equation 5. Rearranging terms gives:

$$2 \log(255\sigma_i) = (p - \mu_{i_{2D}}) \Sigma_{i_{2D}}^{-1} (p - \mu_{i_{2D}})^T. \quad (9)$$

We can rewrite:

$$p = \begin{pmatrix} p_x \\ p_y \end{pmatrix}, \mu_{i_{2D}} = \begin{pmatrix} \mu_x \\ \mu_y \end{pmatrix}, \Sigma_{i_{2D}}^{-1} = \begin{pmatrix} a & b \\ b & c \end{pmatrix}. \quad (10)$$

Specifying threshold t and centered coordinates x_d and y_d :

$$t = 2 \log(255\sigma_i), \quad (11)$$

$$x_d = p_x - \mu_x, \quad (12)$$

$$y_d = p_y - \mu_y, \quad (13)$$

gives the pixel extent with coordinates x_d and y_d that satisfy the ellipse equation:

$$t = ax_d^2 + 2bx_dy_d + cy_d^2. \quad (14)$$

Our approach uses this pixel extent to reduce the number of tiles contained in the Gaussian-to-tile mappings for each Gaussian. We propose two methods for computing precise tile intersections. First, our **SnugBox** algorithm produces a tight bounding box around each Gaussian. Second, our **AccuTile** algorithm extends it to identify the exact set of tiles intersected by the Gaussian.

4.1.1. SnugBox

Our SnugBox method uses this elliptical extent to compute an axis-aligned bounding box that more precisely identifies tiles intersected by Gaussian \mathcal{G}_i . To derive this bounding box, we rearrange Equation 14 to solve for y_d :

$$y_d = \frac{-bx_d \pm \sqrt{(b^2 - ac)x_d^2 + tc}}{c}. \quad (15)$$

To find the y -coordinate bounding box edges y_{\min} and y_{\max} , we identify the values of x_d where $\partial y_d / \partial x_d = 0$. We refer to these x_d values as $x_{d_{args}}$ to specify that they are the $\arg \min y_d$ and $\arg \max y_d$ values. Differentiating Equation 15 and solving for $x_{d_{args}}$ gives:

$$x_{d_{args}} = \pm \sqrt{\frac{-b^2t}{(b^2 - ac)a}}. \quad (16)$$

Substituting $x_{d_{args}}$ into Equation 15 and adding μ_y gives y_{\min} and y_{\max} . Due to the symmetry of Equation 14, we can find the x -coordinate bounding box edges x_{\min} and x_{\max} by swapping y_d and x_d and constants a and c to rewrite Equations 15 and 16 in terms of x_d and $y_{d_{args}}$.

After the bounding box edges are identified, our method follows 3D-GS and converts these edges to tile indices by dividing by tile size, rounding, and clipping to the image boundary. As depicted in Figure 2, Snugbox can produce a significantly tighter bounding box than 3D-GS. Meanwhile, its computational overhead is small as it performs a constant number of operations and is only called twice in the rendering pipeline – once to count the Gaussians intersecting tiles in `preprocess` and once to populate the Gaussian-to-tile arrays in `duplicateWithkeys`. Table 1 reports that SnugBox improves the efficiency of all downstream functions and produces an average overall speed-up of $1.82\times$.

4.1.2. AccuTile

Our AccuTile method, outlined in Algorithm 1, extends SnugBox to identify the exact tiles intersected by the Gaussian. It takes as input the tight bounding box produced by Snugbox and its rectangular tile extent – depicted as the blue box and yellow tiles, respectively, in Figure 2b. Depending on which dimension is smaller, AccuTile then processes either the rows or columns of this tile extent to determine the exact tiles that intersect the Gaussian. Specifically, we identify the minimum and maximum extent of the ellipse within a given row or column, then convert those points to

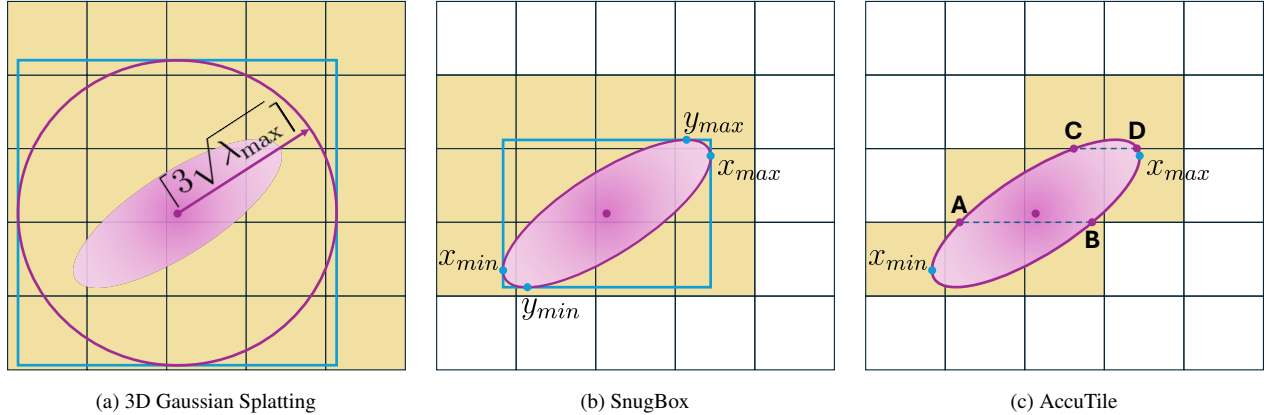


Figure 2. **Gaussian tile allocation by method.** (a) 3D Gaussian Splatting allocates a Gaussian to a tile when that tile **intersects** the **square** inscribing the **circle** with radius $\lceil 3\sqrt{\lambda_{\max}} \rceil$ defined in Equation 8. (b) Our SnugBox method allocates a Gaussian to a tile when that tile **intersects** the tight **bounding box** defined by the axis-aligned minima and maxima of the **ellipse** given by Equation 14. (c) Our AccuTile method allocates a Gaussian to a tile only if that tile **intersects** the **ellipse** via Algorithm 1, which computes the minimum and maximum tiles by iterating over the shorter side of the rectangular tile extent given by SnugBox. In this example, our AccuTile algorithm iterates over the tile rows; the only points that are processed are x_{\min} , x_{\max} , **A**, **B**, **C**, and **D**.

the corresponding touched tiles. All tiles between the minimum and maximum tiles intersect the ellipse.

AccuTile’s key insight is that calculating the minimum and maximum extent of the ellipse within each row or column requires computing only two points per iteration. The only possible inflection points of the elliptical curve are the bounding box minimum and maximum points identified by Snugbox. If one or both of these points lie within the tile row or column, then they represent the minimum or maximum extent of the ellipse there. If neither point is within the row or column, then the points along that boundary side are monotonically decreasing or increasing – the minimum or maximum point must lie on one of the boundary lines of that row or column. Since the boundary of the last row or column is shared with the next one, we only need to compute the intersection of the ellipse with the next boundary line in each iteration. Thus, our AccuTile algorithm counts tiles in time proportional to the shorter side of the tile extent and processes tiles in time proportional to the tile count.

Figure 2 illustrates how Accutile restricts the tight **bounding box** produced by SnugBox to the exact tiles that the Gaussian touches. The **tile extent rows** from Snugbox, shown in Figure 2b, are processed starting from the bottom. The **lower tile row boundary** falls below the **bounding box**, so no initial intersection is computed. The **upper boundary** lies below the top of the **bounding box**, so intersection points **A** and **B** are calculated using Equation 15. x_{\min} is assigned as this row’s minimum ellipse extent e_{\min} because it lies within it, and **B** is assigned as its maximum ellipse extent e_{\max} because it is the maximal point. Consequently, this row’s **tile extent** is from the tile containing x_{\min} to the tile containing **B**. For the next row, we keep points **A** and **B**

and compute upper boundary points **C** and **D**. **A** and x_{\max} are assigned as the row’s e_{\min} and e_{\max} , and the tiles containing them are its **tile extent**. Finally, for the last row, **C** and **D** are kept; no additional points are computed because the row’s upper boundary is above the **bounding box**. Thus, the **tile extent** of this row is between **C** and **D**.

The number of tiles is further reduced from Figure 2b to Figure 2c, much less than the original 3D-GS method in Figure 2a. In Table 1, we report that AccuTile further accelerates all downstream functions, culminating in an average overall speed-up of $1.99\times$.

4.2. Efficient Pruning

PUP 3D-GS [11] is a pruning method that quantifies the sensitivity of each Gaussian to training views, removing a set percentage with the lowest sensitivities. Sensitivity is computed by approximating the Hessian of the L_2 loss:

$$H = \nabla_{\mathcal{G}}^2 L_2 = \sum_{\phi \in \mathcal{P}_{gt}} \nabla_{\mathcal{G}} I_{\mathcal{G}}(\phi) \nabla_{\mathcal{G}} I_{\mathcal{G}}(\phi)^T, \quad (17)$$

where $\nabla_{\mathcal{G}} I_{\mathcal{G}}(\phi)$ is the gradient over all Gaussian parameters on the rendered image $I_{\mathcal{G}}$ for pose ϕ . H is shown to be exact when the L_1 residual error vanishes [11].

A per-Gaussian sensitivity can be derived by splitting H into the block diagonal elements that only capture inter-Gaussian parameter relationships:

$$H_i = \sum_{\phi \in \mathcal{P}_{gt}} \nabla_{\mathcal{G}_i} I_{\mathcal{G}}(\phi) \nabla_{\mathcal{G}_i} I_{\mathcal{G}}(\phi)^T, \quad (18)$$

where $\nabla_{\mathcal{G}_i}$ is the gradient with respect to only \mathcal{G}_i . This measures the sensitivity of the L_2 loss with respect to Gaussian \mathcal{G}_i , assuming all other Gaussians are held constant.

Algorithm 1 The AccuTile Algorithm. For simplicity, the algorithm outlined here is applied to the rows of the Snug-Box tile extent bounding box, matching the example in Figure 2c. In practice, it is applied along the smaller side of the tile extent. The subscripts t , b , l , and r represent the *top*, *bottom*, *left*, and *right* sides, respectively.

Require: Ellipse \mathbf{E} ▷ Eq. 14
Require: SnugBox Bounding Box \mathbf{B}
Require: SnugBox Tile Extent Rectangle \mathbf{R}
Initialize: Tile count $\mathbf{C} \leftarrow 0$
 $\text{line}_{\min} \leftarrow \mathbf{R}_b$
if $\text{line}_{\min} \geq \mathbf{B}_b$ **then**
 $\mathbf{i}_{\min} \leftarrow \text{Intersections}(\text{line}_{\min}, \mathbf{E})$ ▷ Eq. 15
end if
 $\mathbf{C} \leftarrow 0$
for row \mathbf{r} **in** \mathbf{R} **do**
 $\text{line}_{\max} \leftarrow \mathbf{r}_t$
 if $\text{line}_{\max} \leq \mathbf{B}_t$ **then**
 $\mathbf{i}_{\max} \leftarrow \text{Intersections}(\text{line}_{\max}, \mathbf{E})$ ▷ Eq. 15
 end if
 $\mathbf{e}_{\min} \leftarrow \mathbf{B}_l$ **if** \mathbf{B}_l **in** \mathbf{r} **else** $\min(\mathbf{i}_{\min}, \mathbf{i}_{\max})$
 $\mathbf{e}_{\max} \leftarrow \mathbf{B}_r$ **if** \mathbf{B}_r **in** \mathbf{r} **else** $\max(\mathbf{i}_{\min}, \mathbf{i}_{\max})$
 $\text{tile}_{\min}, \text{tile}_{\max} \leftarrow \text{Convert}(\mathbf{e}_{\min}, \mathbf{e}_{\max})$
 $\mathbf{C} \leftarrow \mathbf{C} + (\text{tile}_{\max} - \text{tile}_{\min})$
 Process($\text{tile}_{\min}, \text{tile}_{\max}$)
 $\mathbf{i}_{\min} \leftarrow \mathbf{i}_{\max}$
end for
return \mathbf{C}

H_i is again approximated by only using the six mean μ_i and scale s_i parameters to specifically capture geometric sensitivity. The log determinant is taken to provide a representative scalar score U_i :

$$U_i = \log |\nabla_{\mu_i, s_i} I_G \nabla_{\mu_i, s_i} I_G^T|. \quad (19)$$

Using this score, up to 90% of Gaussians can be robustly pruned from the model while retaining high visual quality.

Although PUP 3D-GS touts high compression ratios and rendering speeds, we identify two key drawbacks in its formulation. First, computing the Hessian requires storage proportional to $N \times 36$, where N is the number of Gaussians, when the memory footprint of the 3D-GS model, which has 59 parameters per Gaussian, is proportional to $N \times 59$. While their score works well for post-hoc pruning, it incurs a resource constraint for use during training.

Second, computing the Hessian requires the pixel-wise gradients of μ and s . Since these are 3D parameters of the Gaussian primitives, obtaining their gradients requires

back-propagating through the `render` kernel parallelized per pixel, then back-propagating each Gaussian contributing to that pixel in its thread. This breaks the efficient flow of gradients in 3D-GS, where the per-pixel gradients from the `render` kernel are parallelized and aggregated to the 2D μ_{2D} and Σ_{2D} parameters, which are then parallelized across Gaussians to compute gradients for μ and s .

Our approach builds on PUP 3D-GS by introducing an **efficient pruning score** that we integrate into the 3D-GS training pipeline. Then, we define two distinct modalities for pruning the model during training: **Soft Pruning** occurs during densification in the first 15000 iterations, and **Hard Pruning** is performed after densification is completed after iteration 15000.

4.2.1. Efficient Pruning Score

Our insight is that both drawbacks can be alleviated by reparameterizing the Hessian. Concretely, we express the influence of all spatial parameters of Gaussian \mathcal{G}_i by computing the Hessian approximation with respect to the 2D projected value of \mathcal{G}_i at pixel p , given by $g_i(p)$ in Equation 6. In doing so, the pruning score U_i from Equation 19 can be expressed as:

$$\tilde{U}_i = \log |\nabla_{g_i} I_G \nabla_{g_i} I_G^T|. \quad (20)$$

Since g_i is a scalar and log is monotonically increasing, we can rewrite this score as:

$$\tilde{U}_i = (\nabla_{g_i} I_G)^2. \quad (21)$$

Gradient $\nabla_{g_i} I_G$ is already computed in the backward pass of `render` and can be efficiently squared and aggregated across all pixels. Moreover, the maximum space requirement for this score is proportional to the number of Gaussians N , reducing the storage requirement by $36\times$ and allowing this score to be used during training.

4.2.2. Soft Pruning

To maintain a robust Hessian approximation, we observe that the L_1 loss becomes quite small by iteration 6000 and remains low except after an opacity reset is performed. As such, we augment the densification pipeline to include our Soft Pruning method, where the model is pruned immediately before the three opacity resets at 6000, 9000, and 12000 iterations. Surprisingly, we find that we can set extremely high Soft Pruning ratios – in our experiments, visual fidelity is preserved at 80% pruning.

4.2.3. Hard Pruning

We also observe that the model performance after densification closely matches that of the fully-trained model. The iterations after densification is completed essentially fine-tune the model – we can use them to “refine” the models after pruning like PUP 3D-GS [11] and LightGaussian [6].

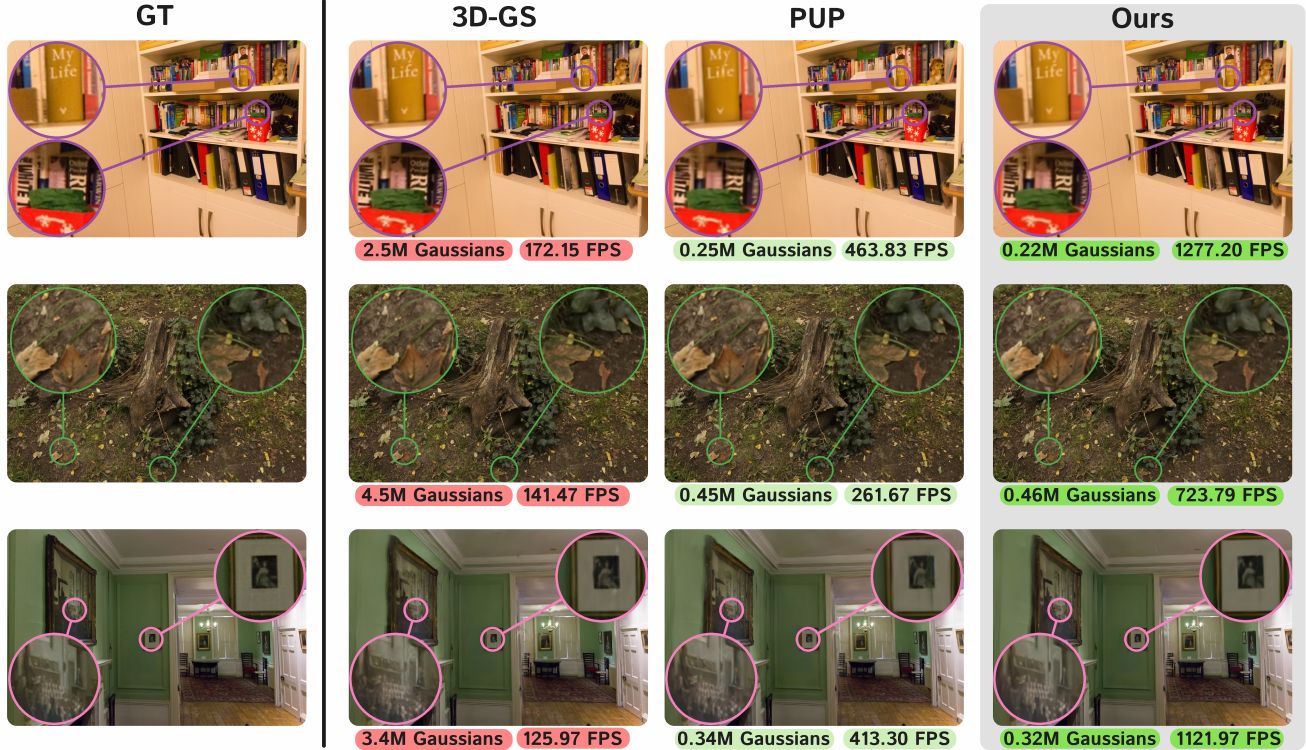


Figure 3. Visual comparison of 3D-GS, PUP 3D-GS, and our method. Notice that, while reaching similar compression ratios to PUP 3D-GS, our Speedy-Splat method delivers vastly faster rendering speeds. Top: *playroom* from the Deep Blending dataset. Middle: *bicycle* from the Mip-NeRF 360 dataset. Bottom: *drjohnson* from the Deep Blending dataset.

In practice, our Hard Pruning method prunes the model by a constant ratio every 3000 iterations starting at iteration 15000. When paired with soft pruning, we Hard Prune 30% of Gaussians in each interval which empirically reduces the total number of Gaussians across scenes by 10.6 \times .

5. Experiments

5.1. Datasets

Our evaluation uses the same set of challenging real-world scenes as 3D-GS [14]. This includes nine Mip-Nerf 360 scenes [3] – four indoor and five outdoor – that each feature a complex central object or area with a detailed background. We also include the outdoor *train* and *truck* scenes from the Tanks & Temples dataset [16] and the indoor *drjohnson* and *playroom* scenes from the Deep Blending dataset [12]. For consistency across experiments, we use the COLMAP pose estimates and sparse point clouds provided by the dataset authors.

5.2. Implementation Details

Our code builds on the differentiable renderer provided by 3D-GS [14] and modifies the Python training pipeline for pruning schedules and execution. To ensure consistent

Table 2. Average Gaussian count, FPS, and training time across all scenes. Ratios for model size compression, rendering speed-up, and training speed-up are reported in (parentheses). The operation in each row is applied **cumulatively** to all of the following rows. The **best** and **second best** value for each metric are color coded.

| Method | # Gaussians ↓ | FPS ↑ | Training Time ↓ |
|---------------|------------------------|----------------------|-----------------------|
| Baseline | 2.93M | 134 | 23.2 |
| +SnugBox | 2.97M | 244 (1.82 \times) | 21.2 (1.09 \times) |
| +AccuTile | 2.97M | 267 (1.99 \times) | 21.0 (1.10 \times) |
| +Soft Pruning | 1.64M (1.79 \times) | 420 (3.14 \times) | 17.5 (1.32 \times) |
| +Hard Pruning | 0.28M (10.6 \times) | 898 (6.71 \times) | 15.7 (1.47 \times) |

and precise timing, all times in Table 1 and FPS values in Tables 2 and 3 are measured using CUDA events at the start and end of the forward rendering procedure. All experiments are conducted on an Nvidia RTX A5000 GPU, and the reported Speedy-Splat results represent the average metrics across three independent runs for each scene.

5.3. Results

5.3.1. Additive method performance

The efficacy of Speedy-Splat is demonstrated by Table 1, where we record the average execution times of each function across all scenes when additively applying

Table 3. Average reported metrics for each pruning method across all scenes in the Mip-NeRF 360 dataset. The *Comp* column reports model size compression in terms of Gaussian count, *FPS* reports rendering speed-up, and *Train* reports training time speed-up, all with respect to the baseline 3D-GS model. PSNR, SSIM, and LPIPS are also recorded. The **best** and **second** best value for each metric are color coded; lossless methods are underlined. Results for the Tanks & Temples and Deep Blending datasets are reported in Appendix A.1.

| Method | Comp \uparrow | FPS \uparrow | Train \uparrow | PSNR \uparrow | SSIM \uparrow | LPIPS \downarrow |
|----------------|--------------------------------|--------------------------------|--------------------------------|-----------------|-----------------|--------------------|
| 3D-GS [14] | 1.00 \times | 1.00 \times | 1.00 \times | 27.55 | 0.814 | 0.222 |
| Trimming [2] | 4.00 \times | - | - | 27.13 | 0.798 | 0.248 |
| Compact [17] | 2.28 \times | 1.07 \times | 0.73 \times | 27.08 | 0.798 | 0.247 |
| EAGLES [10] | 3.68 \times | 1.51 \times | 1.37\times | 26.94 | 0.800 | 0.250 |
| Reducing [23] | 2.33 \times | 1.60 \times | 1.23 \times | 27.10 | 0.809 | 0.226 |
| Light [6] | 2.94 \times | 1.76 \times | - | 27.28 | 0.805 | 0.243 |
| ELMGS [1] | 5.00 \times | 2.69 \times | - | 27.00 | 0.779 | 0.286 |
| PUP [11] | 8.65\times | 2.55 \times | - | 26.83 | 0.792 | 0.268 |
| Mini-Splat [7] | 6.84 \times | 3.20\times | 1.26 \times | 27.34 | 0.822 | 0.217 |
| +SnugBox | 0.99 \times | 1.81 \times | 1.08 \times | 27.55 | 0.814 | 0.221 |
| +AccuTile | 0.99 \times | 1.99 \times | 1.10 \times | 27.57 | 0.814 | 0.221 |
| +Soft Pruning | 1.79 \times | 3.14 \times | 1.30 \times | 27.32 | 0.807 | 0.246 |
| +Hard Pruning | 10.6\times | 6.51\times | 1.45\times | 26.94 | 0.782 | 0.296 |

our methods. SnugBox and AccuTile each introduce minimal additional computation time to preprocess and InclusiveSum. However, limiting the number of tiles touched accelerates all downstream functions, culminating in an overall speed-up of 1.82 \times by SnugBox that is raised to 1.99 \times by AccuTile. Applying soft pruning reduces the runtime of all functions by reducing the number of Gaussians, leading to a 3.14 \times overall speed-up. Finally, performing hard pruning improves overall speed by a whopping 6.71 \times over the baseline 3D-GS model.

5.3.2. Overall Performance

In Figures 1 and 3, we report qualitative results on two outdoor and two indoor scenes from all three datasets. The magnified regions highlight that our method preserves the fine details in the baseline 3D-GS scene and closely models the ground truth view. Despite touting similar compression ratios and rendering nearly identical images, Speedy-Splat achieves over double the FPS of PUP 3D-GS.

Table 3 compares our methods against other methods that reduce the number of Gaussians and increase inference speed using the mean of each metric across all scenes in the Mip-NeRF 360 dataset. The underlined methods are "lossless", meaning that they avoid degrading visual fidelity at all. SnugBox and AccuTile, our lossless methods, improve rendering and training speed while leaving image quality metrics essentially unchanged or slightly better. Our full pipeline, labeled as "+Hard Pruning" boasts the highest compression ratios, rendering speeds, and training speed-ups across all datasets. Furthermore, its image quality metrics are competitive with the other methods.

Table 4. Average metrics across all scenes when using the Speedy-Splat and PUP 3D-GS pruning scores to prune 88.44% of Gaussians using the PUP 3D-GS pipeline. Two rounds of prune-refine are performed on each baseline 3D-GS model, pruning 66% of Gaussians and then fine-tuning for 5,000 iterations in each one. The **best** value for each metric is color coded.

| Method | # Gaussians \downarrow | PSNR \uparrow | SSIM \uparrow | LPIPS \downarrow | FPS \uparrow |
|----------|--------------------------|-----------------|-----------------|--------------------|----------------|
| Baseline | 2.92M | 27.1503 | 0.8296 | 0.2238 | 107.53 |
| PUP [11] | 0.34M | 26.2136 | 0.8044 | 0.2731 | 378.57 |
| Ours | 0.34M | 26.8658 | 0.8022 | 0.2840 | 345.52 |

5.4. Pruning Score Comparison

Although the primary focus of our work is rendering speed, we find that our efficient pruning score, described in Section 4.2, also performs well when applied in other compression pipelines. In Table 4, we ablate our efficient pruning score with the PUP 3D-GS sensitivity score across all scenes in their post-hoc pruning pipeline. Notably, Speedy-Splat’s efficient pruning score outperforms PUP 3D-GS on PSNR and is competitive across the other metrics.

6. Limitations

A limitation of Speedy-Splat is that it produces slightly lower image quality than 3D-GS. However, this degradation is expected at high compression ratios and is also observed in comparable techniques. Additionally, a direct comparison of our efficient pruning score to the PUP 3D-GS pruning score illuminates a slight, yet noticeable, gap in performance. Future work could explore the possibility of another efficient pruning score that delivers higher performance.

7. Conclusion

In this work, we present Speedy-Splat: a new 3D-GS technique that accurately localizes Gaussians during rendering and significantly improves inference speed, model size, and training time. Enhanced localization is achieved by our SnugBox and AccuTile methods, while model size reduction is accomplished by our Soft and Hard Pruning approaches. Together, our Speedy-Splat methods accelerate rendering speed by an average of 6.71 \times , reduce model size by 10.6 \times , and improve training time by 1.47 \times across all scenes from the Mip-NeRF 360, Tanks & Temples, and Deep Blending datasets.

8. Acknowledgements

This work was made possible by the IARPA WRIVA Program, the ONR MURI program, and DAPRA TIAMAT. Commercial support was provided by Capital One Bank, the Amazon Research Award program, and Open Philanthropy. Further support was provided by the National Science Foundation (IIS-2212182), and by the NSF TRAILS Institute (2229885). Zwicker was additionally supported by the National Science Foundation (IIS-2126407).

References

- [1] Muhammad Salman Ali, Sung-Ho Bae, and Enzo Tartaglione. Elmg: Enhancing memory and computation scalability through compression for 3d gaussian splatting. *arXiv preprint arXiv:2410.23213*, 2024. 2, 8, 10
- [2] Muhammad Salman Ali, Maryam Qamar, Sung-Ho Bae, and Enzo Tartaglione. Trimming the fat: Efficient compression of 3d gaussian splats through pruning. *arXiv preprint arXiv:2406.18214*, 2024. 2, 8, 10
- [3] Jonathan T Barron, Ben Mildenhall, Dor Verbin, Pratul P Srinivasan, and Peter Hedman. Mip-nerf 360: Unbounded anti-aliased neural radiance fields. In *Proceedings of the IEEE/CVF Conference on Computer Vision and Pattern Recognition*, pages 5470–5479, 2022. 7
- [4] Anpei Chen, Zexiang Xu, Andreas Geiger, Jingyi Yu, and Hao Su. Tensorf: Tensorial radiance fields. In *European Conference on Computer Vision (ECCV)*, 2022. 1
- [5] Sankeerth Durvasula, Adrian Zhao, Fan Chen, Ruofan Liang, Pawan Kumar Sanjaya, and Nandita Vijaykumar. Distwar: Fast differentiable rendering on raster-based rendering pipelines. *arXiv preprint arXiv:2401.05345*, 2023. 2
- [6] Zhiwen Fan, Kevin Wang, Kairun Wen, Zehao Zhu, Dejia Xu, and Zhangyang Wang. Lightgaussian: Unbounded 3d gaussian compression with 15x reduction and 200+ fps. *arXiv preprint arXiv:2311.17245*, 2023. 1, 2, 6, 8, 10
- [7] Guangchi Fang and Bing Wang. Mini-splatting: Representing scenes with a constrained number of gaussians. *arXiv preprint arXiv:2403.14166*, 2024. 1, 2, 8, 10
- [8] Guofeng Feng, Siyan Chen, Rong Fu, Zimu Liao, Yi Wang, Tao Liu, Zhilin Pei, Hengjie Li, Xingcheng Zhang, and Bo Dai. Flashgs: Efficient 3d gaussian splatting for large-scale and high-resolution rendering. *arXiv preprint arXiv:2408.07967*, 2024. 1, 2
- [9] Henri P. Gavin. The levenberg-marquardt method for non-linear least squares curve-fitting problems c ©. 2013. 2
- [10] Sharath Girish, Kamal Gupta, and Abhinav Shrivastava. Eagles: Efficient accelerated 3d gaussians with lightweight encodings. *arXiv preprint arXiv:2312.04564*, 2023. 2, 8, 10
- [11] Alex Hanson, Allen Tu, Vasu Singla, Mayuka Jayawardhana, Matthias Zwicker, and Tom Goldstein. Pup 3d-gs: Principled uncertainty pruning for 3d gaussian splatting. *arXiv preprint arXiv:2406.10219*, 2024. 1, 2, 4, 5, 6, 8, 10
- [12] Peter Hedman, Julien Philip, True Price, Jan-Michael Frahm, George Drettakis, and Gabriel Brostow. Deep blending for free-viewpoint image-based rendering. *ACM Transactions on Graphics*, 37(6):1–15, 2018. 7
- [13] Lukas Höllein, Aljaž Božič, Michael Zollhöfer, and Matthias Nießner. 3dgs-lm: Faster gaussian-splatting optimization with levenberg-marquardt. *arXiv preprint arXiv:2409.12892*, 2024. 2
- [14] Bernhard Kerbl, Georgios Kopanas, Thomas Leimkühler, and George Drettakis. 3d gaussian splatting for real-time radiance field rendering. *ACM Transactions on Graphics*, 42(4):1–14, 2023. 1, 2, 3, 7, 8, 10
- [15] Diederik P. Kingma and Jimmy Ba. Adam: A method for stochastic optimization. *CoRR*, abs/1412.6980, 2014. 2
- [16] Arno Knapitsch, Jaesik Park, Qian-Yi Zhou, and Vladlen Koltun. Tanks and temples: Benchmarking large-scale scene reconstruction. *ACM Transactions on Graphics*, 36(4):1–13, 2017. 7
- [17] Joo Chan Lee, Daniel Rho, Xiangyu Sun, Jong Hwan Ko, and Eunbyung Park. Compact 3d gaussian representation for radiance field. *arXiv preprint arXiv:2311.13681*, 2023. 2, 8, 10
- [18] Weikai Lin, Yu Feng, and Yuhao Zhu. Rtg: Enabling real-time gaussian splatting on mobile devices using efficiency-guided pruning and foveated rendering. *arXiv preprint arXiv:2407.00435*, 2024. 1, 2
- [19] Xiangrui Liu, Xinju Wu, Pingping Zhang, Shiqi Wang, Zhu Li, and Sam Kwong. Compgs: Efficient 3d scene representation via compressed gaussian splatting. *arXiv preprint arXiv:2404.09458*, 2024. 2
- [20] Ben Mildenhall, Pratul P Srinivasan, Matthew Tancik, Jonathan T Barron, Ravi Ramamoorthi, and Ren Ng. Nerf: Representing scenes as neural radiance fields for view synthesis. *Communications of the ACM*, 65(1):99–106, 2021. 1
- [21] Thomas Müller, Alex Evans, Christoph Schied, and Alexander Keller. Instant neural graphics primitives with a multiresolution hash encoding. *ACM Trans. Graph.*, 41(4):102:1–102:15, 2022. 1
- [22] Michael Niemeyer, Fabian Manhardt, Marie-Julie Rakotosaona, Michael Oechsle, Daniel Duckworth, Rama Gosula, Keisuke Tateno, John Bates, Dominik Kaeser, and Federico Tombari. Radsplat: Radiance field-informed gaussian splatting for robust real-time rendering with 900+ fps. *arXiv preprint arXiv:2403.13806*, 2024. 1, 2
- [23] Panagiotis Papantonakis, Georgios Kopanas, Bernhard Kerbl, Alexandre Lanvin, and George Drettakis. Reducing the memory footprint of 3d gaussian splatting. *Proceedings of the ACM on Computer Graphics and Interactive Techniques*, 7(1):1–17, 2024. 2, 8, 10
- [24] Fernando Rivas-Manzanique, Jorge Sierra-Acosta, Adrian Penate-Sanchez, Francesc Moreno-Noguer, and Angela Ribeiro. Nerflight: Fast and light neural radiance fields using a shared feature grid. In *Proceedings of the IEEE/CVF Conference on Computer Vision and Pattern Recognition (CVPR)*, pages 12417–12427, 2023. 1
- [25] Saswat Mallick and Rahul Goel, Bernhard Kerbl, Francisco Vicente Carrasco, Markus Steinberger, and Fernando De La Torre. Taming 3dgs: High-quality radiance fields with limited resources. In *SIGGRAPH Asia 2024 Conference Papers*, 2024. 2
- [26] Matthias Zwicker, Hanspeter Pfister, Jeroen Van Baar, and Markus Gross. Ewa splatting. *IEEE Transactions on Visualization and Computer Graphics*, 8(3):223–238, 2002. 3

A. Appendix

A.1. Additional Datasets Evaluation

Table 5 and Table 6 present the average reported metrics for each pruning method across all scenes in the Tanks & Temples and Deep Blending datasets, respectively. The *Comp* column reports model size compression in terms of Gaussian count, *FPS* reports rendering speed-up, and *Train* reports training time speed-up, all with respect to the baseline 3D-GS model. PSNR, SSIM, and LPIPS are also recorded. The **best** and **second** best value for each metric are color coded; lossless methods are underlined.

Table 5. Average reported metrics for each pruning method across all scenes in the Tanks & Temples dataset.

| Method | Comp \uparrow | FPS \uparrow | Train \uparrow | PSNR \uparrow | SSIM \uparrow | LPIPS \downarrow |
|----------------|-----------------|----------------|------------------|-----------------|-----------------|--------------------|
| 3D-GS [14] | 1.00 \times | 1.00 \times | 1.00 \times | 23.70 | 0.849 | 0.178 |
| Trimming [2] | 4.00 \times | - | - | 23.69 | 0.831 | 0.210 |
| Compact [17] | 2.19 \times | 1.16 \times | 0.76 \times | 23.32 | 0.831 | 0.201 |
| EAGLES [10] | - | 1.73 \times | 1.19 \times | 23.10 | 0.820 | 0.220 |
| Reducing [23] | 2.56 \times | 1.91 \times | 1.27 \times | 23.57 | 0.840 | 0.188 |
| Light [6] | 2.94 \times | 1.97 \times | - | 23.11 | 0.817 | 0.231 |
| ELMGS [1] | 5.00 \times | 4.05 \times | - | 23.90 | 0.825 | 0.233 |
| PUP [11] | 10.0 \times | 4.00 \times | - | 22.72 | 0.801 | 0.244 |
| Mini-Splat [7] | 9.20 \times | - | - | 23.18 | 0.835 | 0.202 |
| +SnugBox | 0.99 \times | 1.61 \times | 1.11 \times | 23.69 | 0.849 | 0.178 |
| +AccuTile | 0.99 \times | 1.67 \times | 1.12 \times | 23.73 | 0.849 | 0.177 |
| +Soft Pruning | 1.69 \times | 2.48 \times | 1.36 \times | 23.54 | 0.841 | 0.201 |
| +Hard Pruning | 10.1 \times | 6.30 \times | 1.58 \times | 23.45 | 0.821 | 0.241 |

Table 6. Average reported metrics for each pruning method across all scenes in the Deep Blending dataset.

| Method | Comp \uparrow | FPS \uparrow | Train \uparrow | PSNR \uparrow | SSIM \uparrow | LPIPS \downarrow |
|----------------|-----------------|----------------|------------------|-----------------|-----------------|--------------------|
| 3D-GS [14] | 1.00 \times | 1.00 \times | 1.00 \times | 29.09 | 0.886 | 0.288 |
| Trimming [2] | 1.33 \times | - | - | 29.43 | 0.897 | 0.267 |
| Compact [17] | 2.65 \times | 1.37 \times | 0.79 \times | 29.79 | 0.901 | 0.258 |
| EAGLES [10] | - | 1.30 \times | 1.31 \times | 29.92 | 0.900 | 0.250 |
| Reducing [23] | 2.86 \times | 1.79 \times | 1.27 \times | 29.63 | 0.902 | 0.249 |
| Light [6] | - | - | - | - | - | - |
| ELMGS [1] | 5.00 \times | 4.15 \times | - | 29.24 | 0.894 | 0.273 |
| PUP [11] | 10.0 \times | 4.51 \times | - | 28.85 | 0.881 | 0.301 |
| Mini-Splat [7] | 8.06 \times | - | - | 29.98 | 0.908 | 0.253 |
| +SnugBox | 0.97 \times | 2.11 \times | 1.12 \times | 29.18 | 0.886 | 0.287 |
| +AccuTile | 0.97 \times | 2.32 \times | 1.13 \times | 29.12 | 0.885 | 0.288 |
| +Soft Pruning | 1.86 \times | 3.56 \times | 1.41 \times | 29.29 | 0.889 | 0.296 |
| +Hard Pruning | 11.1 \times | 7.46 \times | 1.57 \times | 29.32 | 0.887 | 0.311 |

A.2. Per-Scene Metrics

PSNR, SSIM, LPIPS, FPS, and training times for each scene from the Mip-NeRF 360, Tanks&Temples, and Deep Blending datasets that was used in 3D-GS [14] are recorded in Tables 7, 8, 9, 10, and Table 11, respectively. The operation in each row is applied **cumulatively** to all of the following rows.

Table 7. PSNR \uparrow on each scene after cumulatively applying each function.

| Method | Mip-NeRF 360 | | | | | | | | | Tanks & Temples | | Deep Blending | |
|---------------|--------------|--------|---------|---------|--------|---------|-------|-------|----------|-----------------|-------|---------------|----------|
| | bicycle | bonsai | counter | flowers | garden | kitchen | room | stump | treehill | train | truck | drjohnson | playroom |
| Baseline | 25.10 | 32.42 | 29.14 | 21.41 | 27.31 | 31.49 | 31.66 | 26.78 | 22.62 | 22.01 | 25.40 | 28.18 | 30.00 |
| +SnugBox | 25.12 | 32.36 | 29.09 | 21.45 | 27.31 | 31.61 | 31.70 | 26.78 | 22.54 | 21.97 | 25.41 | 28.27 | 30.09 |
| +AccuTile | 25.13 | 32.42 | 29.13 | 21.43 | 27.33 | 31.65 | 31.68 | 26.80 | 22.58 | 22.00 | 25.45 | 28.23 | 30.00 |
| +Soft Pruning | 25.09 | 31.91 | 28.74 | 21.35 | 27.16 | 30.83 | 31.32 | 26.88 | 22.57 | 21.74 | 25.34 | 28.44 | 30.14 |
| +Hard Pruning | 24.78 | 31.29 | 28.28 | 21.21 | 26.70 | 29.91 | 30.99 | 26.79 | 22.51 | 21.71 | 25.20 | 28.50 | 30.14 |

Table 8. SSIM \uparrow on each scene after cumulatively applying each function.

| Method | Mip-NeRF 360 | | | | | | | | | Tanks & Temples | | Deep Blending | |
|---------------|--------------|--------|---------|---------|--------|---------|-------|-------|----------|-----------------|-------|---------------|----------|
| | bicycle | bonsai | counter | flowers | garden | kitchen | room | stump | treehill | train | truck | drjohnson | playroom |
| Baseline | 0.747 | 0.948 | 0.916 | 0.589 | 0.857 | 0.933 | 0.927 | 0.770 | 0.636 | 0.815 | 0.883 | 0.880 | 0.891 |
| +SnugBox | 0.749 | 0.948 | 0.916 | 0.591 | 0.857 | 0.933 | 0.928 | 0.771 | 0.636 | 0.815 | 0.883 | 0.880 | 0.892 |
| +AccuTile | 0.749 | 0.948 | 0.916 | 0.590 | 0.857 | 0.933 | 0.927 | 0.771 | 0.637 | 0.816 | 0.883 | 0.879 | 0.891 |
| +Soft Pruning | 0.741 | 0.941 | 0.904 | 0.582 | 0.848 | 0.921 | 0.920 | 0.776 | 0.630 | 0.803 | 0.878 | 0.884 | 0.893 |
| +Hard Pruning | 0.704 | 0.927 | 0.878 | 0.561 | 0.815 | 0.894 | 0.905 | 0.765 | 0.590 | 0.773 | 0.868 | 0.882 | 0.892 |

Table 9. LPIPS \downarrow on each scene after cumulatively applying each function.

| Method | Mip-NeRF 360 | | | | | | | | | Tanks & Temples | | Deep Blending | |
|---------------|--------------|--------|---------|---------|--------|---------|-------|-------|----------|-----------------|-------|---------------|----------|
| | bicycle | bonsai | counter | flowers | garden | kitchen | room | stump | treehill | train | truck | drjohnson | playroom |
| Baseline | 0.244 | 0.183 | 0.185 | 0.359 | 0.122 | 0.118 | 0.200 | 0.242 | 0.346 | 0.208 | 0.147 | 0.291 | 0.284 |
| +SnugBox | 0.241 | 0.183 | 0.185 | 0.358 | 0.122 | 0.117 | 0.199 | 0.241 | 0.345 | 0.208 | 0.147 | 0.291 | 0.284 |
| +AccuTile | 0.242 | 0.183 | 0.185 | 0.359 | 0.122 | 0.117 | 0.199 | 0.241 | 0.344 | 0.207 | 0.147 | 0.292 | 0.284 |
| +Soft Pruning | 0.271 | 0.197 | 0.212 | 0.379 | 0.147 | 0.141 | 0.222 | 0.258 | 0.390 | 0.237 | 0.165 | 0.297 | 0.295 |
| +Hard Pruning | 0.333 | 0.231 | 0.260 | 0.419 | 0.213 | 0.198 | 0.260 | 0.288 | 0.463 | 0.291 | 0.191 | 0.313 | 0.308 |

Table 10. FPS \uparrow on each scene after cumulatively applying each function. Speed-ups \uparrow are recorded in (parentheses).

| Method | Mip-NeRF 360 | | | | | | | | | Tanks & Temples | | Deep Blending | |
|---------------|-------------------------|-------------------------|-------------------------|--------------------------|-------------------------|-------------------------|-------------------------|--------------------------|-------------------------|-------------------------|--------------------------|-------------------------|--------------------------|
| | bicycle | bonsai | counter | flowers | garden | kitchen | room | stump | treehill | train | truck | drjohnson | playroom |
| Baseline | 71 | 201 | 142 | 126 | 164 | 91 | 117 | 172 | 140 | 141 | 200 | 138 | 185 |
| +SnugBox | 154 (2.15 \times) | 358 (1.78 \times) | 276 (1.95 \times) | 301 (2.39 \times) | 267 (1.62 \times) | 146 (1.60 \times) | 197 (1.68 \times) | 335 (1.95 \times) | 301 (2.15 \times) | 228 (1.61 \times) | 320 (1.60 \times) | 247 (1.79 \times) | 282 (1.53 \times) |
| +AccuTile | 168 (2.35 \times) | 413 (2.05 \times) | 330 (2.33 \times) | 332 (2.64 \times) | 285 (1.73 \times) | 155 (1.70 \times) | 221 (1.89 \times) | 378 (2.20 \times) | 315 (2.25 \times) | 248 (1.75 \times) | 343 (1.71 \times) | 272 (1.97 \times) | 294 (1.59 \times) |
| +Soft Pruning | 241 (3.37 \times) | 601 (2.99 \times) | 505 (3.56 \times) | 497 (3.95 \times) | 419 (2.55 \times) | 255 (2.80 \times) | 425 (3.63 \times) | 612 (3.56 \times) | 549 (3.92 \times) | 379 (2.68 \times) | 518 (2.59 \times) | 423 (3.06 \times) | 477 (2.58 \times) |
| +Hard Pruning | 662 (9.25 \times) | 978 (4.87 \times) | 842 (5.94 \times) | 1122 (8.91 \times) | 825 (5.02 \times) | 640 (7.03 \times) | 809 (6.90 \times) | 1277 (7.42 \times) | 942 (6.73 \times) | 724 (5.12 \times) | 1392 (6.95 \times) | 957 (6.93 \times) | 1149 (6.21 \times) |

Table 11. Training time \downarrow in minutes on each scene after cumulatively applying each function. Speed-ups \uparrow are recorded in (parentheses).

| Method | Mip-NeRF 360 | | | | | | | | | Tanks & Temples | | Deep Blending | |
|---------------|--------------------------|--------------------------|--------------------------|--------------------------|--------------------------|--------------------------|--------------------------|--------------------------|--------------------------|-------------------------|--------------------------|--------------------------|--------------------------|
| | bicycle | bonsai | counter | flowers | garden | kitchen | room | stump | treehill | train | truck | drjohnson | playroom |
| Baseline | 31.9 | 20.4 | 24.1 | 24.1 | 32.3 | 27.8 | 23.7 | 24.1 | 24.2 | 11.1 | 13.4 | 24.8 | 19.5 |
| +SnugBox | 28.2 (1.13 \times) | 19.2 (1.07 \times) | 21.8 (1.11 \times) | 22.7 (1.06 \times) | 29.9 (1.08 \times) | 25.8 (1.08 \times) | 21.4 (1.11 \times) | 22.9 (1.05 \times) | 22.4 (1.08 \times) | 9.8 (1.13 \times) | 12.3 (1.09 \times) | 21.7 (1.14 \times) | 17.8 (1.09 \times) |
| +AccuTile | 27.8 (1.15 \times) | 19.0 (1.08 \times) | 21.3 (1.13 \times) | 22.6 (1.07 \times) | 29.4 (1.10 \times) | 25.5 (1.09 \times) | 21.1 (1.12 \times) | 22.7 (1.06 \times) | 22.3 (1.08 \times) | 9.7 (1.14 \times) | 12.2 (1.09 \times) | 21.5 (1.15 \times) | 17.7 (1.10 \times) |
| +Soft Pruning | 23.1 (1.38 \times) | 17.0 (1.20 \times) | 18.6 (1.30 \times) | 19.5 (1.23 \times) | 23.2 (1.39 \times) | 20.3 (1.37 \times) | 18.3 (1.30 \times) | 19.3 (1.25 \times) | 18.9 (1.27 \times) | 8.3 (1.33 \times) | 9.7 (1.38 \times) | 17.3 (1.43 \times) | 14.2 (1.37 \times) |
| +Hard Pruning | 19.7 (1.62 \times) | 16.0 (1.28 \times) | 17.7 (1.36 \times) | 17.5 (1.38 \times) | 20.3 (1.59 \times) | 18.7 (1.49 \times) | 16.9 (1.40 \times) | 17.1 (1.41 \times) | 16.9 (1.43 \times) | 7.2 (1.55 \times) | 8.3 (1.61 \times) | 15.3 (1.62 \times) | 12.8 (1.52 \times) |